Applied Catalysis B: Environmental 113–114 (2012) 61–71

Contents lists available at SciVerse ScienceDirect

Applied Catalysis B: Environmental

journal homepage: www.elsevier.com/locate/apcatb

The effect of infrared light on visible light photocatalytic activity: An intensive contrast between Pt-doped TiO_2 and N-doped TiO_2

Caixia Feng[a,b,*], Yan Wang[a], Jingwei Zhang[a], Laigui Yu[a], Deliang Li[b], Jianjun Yang[a], Zhijun Zhang[a]

[a] Key Laboratory for Special Functional Materials of the Ministry of Education, Henan University, Kaifeng 475004, China
[b] Institute of Environmental and Analytical Sciences, College of Chemistry and Chemical Engineering, Henan University, Kaifeng 475004, China

ARTICLE INFO

Article history:
Received 20 July 2011
Received in revised form
15 September 2011
Accepted 21 September 2011
Available online 28 September 2011

Keywords:
Titanium dioxide
Platinum-doped
Nitrogen-doped
Oxygen vacancy
Infrared light

ABSTRACT

Pt-doped TiO_2 and N-doped TiO_2 were prepared, using nanotubular titanic acid as precursor, by wet impregnation and NH_3-heating method, respectively. Both Pt-doped and N-doped TiO_2 show an apparent photocatalytic oxidation of propylene under visible light irradiation. The origin of visible light sensitization was ascribed to the intra-band contributed by the formation of single-electron-trapped oxygen vacancies, while dopants platinum or nitrogen play a role not only in suppressing the recombination of photoinduced electrons and holes but also in increasing the ability of visible light absorption of TiO_2. The visible light photocatalytic activity of Pt-doped TiO_2 can be greatly improved by additional infrared light irradiation, while visible-light-active N-doped TiO_2 has no such phenomenon. Infrared light per se is unable to excite Pt-doped TiO_2 catalyst to initiate photocatalytic reaction, but the strong interaction between platinum and oxygen vacancies resulted in absorption peaks at 800–900 nm, resulting in a giant enhancement in visible light photocatalytic activity of Pt-doped TiO_2 in the presence of infrared light irradiation because the formed heterojunctions between dopants Pt and TiO_2 may function as thermal catalytic sites. The influences of reaction temperatures on visible light photoactivity of both Pt-doped and N-doped TiO_2 were studied. It was found that both C_3H_6 removal and CO_2 selectivity over Pt-doped TiO_2 were increased with increasing the reaction temperature, while it was inert for N-doped TiO_2.

1. Introduction

Titanium dioxide based photocatalysts have been regarded as the most promising materials in the field of water splitting [1–4], solar energy conversion [5–7] and environmental remediation [8–12] because of its toxicity-free, high oxidative power, lower cost and long-term chemical stability. However, its practical applications are strongly limited due to the relatively large band gap of TiO_2 (3.2 eV for the anatase phase and 3.0 eV for the rutile phase), which is only sensitive to ultraviolet (UV) light accounting for only 5% of the natural solar light. Generally speaking, UV light source is unexpected because it usually consumes electricity energy and generates ozone gas harming to human health. From energy saving and utilization point of view, solar energy is the most favorable light source for a photocatalytic system. In order to utilize visible light even indoor light more efficiently, cation doping has been attempted as the first generation strategy to obtain visible-light-active (VLA) TiO_2 and then anion doping as the second strategy [13]. Among cation doping of TiO_2, platinized TiO_2 has been widely studied and regarded as the most commonly applied techniques to improve the overall photocatalytic performance. Pt-dopants play a role not only in increasing formation of hydroxyl radicals and oxygen species by trapping photoinduced electrons but also provide thermal catalytic sites for target degradants and reaction intermediates [14–19]. However, Pt-dopants sometimes showed negatively photocatalytic degradation activity which may result from the occupying of TiO_2 surface active sites by excess Pt-dopants [20,21], undesired presence of inactive Pt oxidation state depending on the preparation procedure [14,15,22–24], and Pt-promoted recombination of photo-generated electrons and holes [21,25,26]. In parallel, in the past decade, anion doping especially nitrogen doping, with the possibility to significantly enhance the visible light absorption and photocatalytic activity of TiO_2, is of particular interest since Asahi et al. obtained a VLA $TiO_{2-x}N_x$ films by sputtering the TiO_2 target in a N_2(40%)/Ar gas mixture in 2001 [27]. Afterwards, many preparation methods have been reported for N-doped TiO_2 such as calcination or magnetron sputtering of TiO_2 target under special gas [8,27–32], sol–gel [33,34], ion implantation of powder or nanotubular TiO_2 [35–38] and direct oxidation of TiN [39]. Such as-prepared N-doped TiO_2 showed an

* Corresponding author at: Institute of Environmental and Analytical Sciences, College of Chemistry and Chemical Engineering, Henan University, Kaifeng 475004, China. Tel.: +86 378 2868833; fax: +86 378 3881589.
E-mail address: caixia8079@henu.edu.cn (C. Feng).

0926-3373/$ – see front matter © 2011 Elsevier B.V. All rights reserved.
doi:10.1016/j.apcatb.2011.09.027

apparently enhanced visible light photocatalytic activity compared with pristine undoped TiO_2. However, both the role of N-dopants on enhanced visible light photocatalytic activity and the mechanism of the photoactivity of N-doped TiO_2 in visible light region are still an open subject of controversy. Aiming to reveal the origin of visible light sensitization of N-doped TiO_2, we prepared N-doped TiO_2 by heat-treatment of P25 (Degussa) and nanotubular titanic acid (denoted as NTA) in flowing NH_3 [40,41]. Our results indicated that the visible light absorption and photocatalytic activity of N-doped TiO_2 is closely correlated to the presence of single-electron-trapped oxygen vacancies (denoted as SETOVs) formed during the heat treatment process in flowing NH_3. It was suggested that the visible light photocatalytic activity of N-doped TiO_2 is co-determined by the generation of SETOVs in TiO_2 matrix and the existence of doped-N on the surface. This, at least seemingly, may be more rational, since Serpone et al. systematically studied the absorption spectral features of pristine undoped and doped TiO_2 specimens and proposed that the enhanced absorption bands seen in the visible spectral region were associated with oxygen vacancies (i.e., *F*-type color centers) [42]. Moreover, our results suggested that the concentration of SETOV varied with varying precursors for N-doping. Annealing NTA in flowing NH_3 caused phase transformation from orthorhombic of NTA to anatase TiO_2 and generated a large amount of SETOV, while the heat-treatment of P25 in flowing NH_3 leads to a small quantity of SETOV. By comparing the difference between the visible light photocatalytic activity of N-doped TiO_2 prepared from different precursors and the concentration of SETOV, it was proposed that NTA is one of the most promising materials for designing VLA photocatalyst [41].

So far numerous papers are available about the improved visible light photocatalytic activity of Pt/TiO_2 and N-doped TiO_2, though their mechanisms of visible light response are still under controversy. However, few work put their eyes on the comparison between the visible light photocatalytic activity under the same conditions of Pt/TiO_2 and N-doped TiO_2. In the present paper, samples Pt/TiO_2 and N-doped TiO_2 prepared by wet impregnation and NH_3-heating method, respectively, together with corresponding visible light photocatalytic degradation of propylene under the same reaction conditions are systematically studied. It was suggested that the visible light sensitization was originated from the intra-band offered by the formation of SETOVs, while dopants play a role not only in preventing photoinduced electrons and holes from recombination but also in increasing the ability of visible light absorption of TiO_2. Furthermore, we researched the effect of the additional infrared light irradiation on the visible light photocatalytic activity, which, to the best of our knowledge, has not been reported elsewhere. Interestingly, an intensive contrast between the effect of infrared light on the visible light photocatalytic activity of Pt/TiO_2 and N-doped TiO_2 was obvious observed. The visible light photocatalytic activity of Pt-doped TiO_2 can be greatly improved by additional infrared light irradiation, while VLA N-doped TiO_2 has no such phenomenon. To reveal the origination, the influence of reaction temperatures on visible light photoactivity of both Pt-doped and N-doped TiO_2 was studied and the results showed that both C_3H_6 removal and CO_2 selectivity over Pt-doped TiO_2 were increased with increasing the reaction temperature, while it was inert for N-doped TiO_2. Therefore, it is inferred that Pt-dopants may also provide thermal catalytic sites so that infrared light irradiation can accelerate the transfer of photoinduced electrons so as to promote the separation efficiency of photoinduced electrons and holes pairs, while N-dopants has no such function. As such, the results present here represent a significant new finding that Pt-doped TiO_2 can utilize the lower-energy tails of the solar spectrum and showed a better improved visible light photocatalytic activity, while N-doped TiO_2 has a better photocatalytic performance when using visible light only.

2. Experimental

2.1. Catalyst preparation

2.1.1. Preparation of nanotubular titanic acid (denoted as NTA)

NTA was prepared according to the method reported elsewhere [8]. Typically, the preparing procedure of NTA is as follows: 3 g of P25-TiO_2 reacted with 10 M NaOH solution under magnetic stirring at 120 °C for 24 h. When the dispersion naturally cooled down to room temperature, it was washed with de-ionized water to a pH of ca. 7.0–8.0, and then immersed in 0.1 M HCl solution for 5 h under magnetic stirring, washed again with de-ionized water to remove Cl^- followed by drying under vacuum at room temperature, yielding ca. 3 g of NTA. Because the chemicals used were reagent grade, we denoted the as-prepared NTA as NTA-R.

Moreover, we have enlarged the preparation scale of NTA up to kilograms level. The preparing procedure was similar to the above. However, P25-TiO_2 was replaced by titanium white and all the chemicals used were industry grade. In contrast to NTA-R, we denoted the product as NTA-I.

2.1.2. Preparation of Pt-doped TiO_2

Pt-doped TiO_2 samples containing 1 wt.%, 3 wt.% and 5 wt.% (mass fraction) Pt were synthesized using wet impregnation method using NTA-R as the precursor. A proper amount of NTA-R was placed in a filter flask attached to a vacuum pump and outgassed for several hours, followed by dropwise addition of a predetermined amount of chloroplatinic acid (H_2PtCl_6) solution from a funnel. Resultant mixture was dried in an infrared-ray oven, oxidized at 400 °C for 3 h, and finally reduced at 200 °C in flowing hydrogen for 2 h yielding target products denoted as 1 wt.% Pt/TiO_2, 3 wt.% Pt/TiO_2, and 5 wt.% Pt/TiO_2.

2.1.3. Preparation of N-doped TiO_2

N-doped TiO_2 samples were prepared by NH_3-heating method reported elsewhere [8]. Briefly, an aliquot of NTA-I was thermally treated in flowing NH_3 at 400 °C, 500 °C and 600 °C for 4 h, respectively, yielding N-TiO_2-400, N-TiO_2-500, and N-TiO_2-600.

2.2. Catalyst characterization

X-ray diffraction (XRD) patterns were measured on an X'Pert Philips diffractometer (Cu Kα radiation; 2θ range 4–90°, step size 0.02°, accelerating voltage 40 kV, applied current 40 mA). Electron spin resonance (ESR) spectra were obtained on a Brüker ESP 300E apparatus (operated in X band: ca. 9.80 kHz) at a field modulation of 100 kHz, an amplitude modulation of 0.2 mT and a microwave power of 10 mW (the measurement was performed at room temperature and in ambient air, without vacuum-pumping). The *g*-tensors of the ESR signals were obtained by setting *g* of diphenyl picryl hydrazyl (DPPH), 2.0036, as reference. Diffuse reflectance spectra (DRS) were obtained on a Shimadzu U-4100 spectrometer, using $BaSO_4$ as a reference. X-ray photoelectron spectra (XPS) were recorded with a Kratos AXIS Ultra spectrometer using monochromatized Al Kα ($h\nu$ = 1486.6 eV) radiation as the excitation source (power 150 W: 15 kV × 10 mA). The binding energy of hydrocarbon (C 1*s*: 284.8 eV) was used as an internal standard for the correction of charging shift. During acquisition of XPS data, the pressure of sample analysis chamber (SAC) was kept below 10^{-8}–10^{-9} torr. Survey spectra and core level spectra were collected at pass energy of 80 eV and 40 eV, respectively.

2.3. Activity test of relevant samples

The photocatalytic activity of Pt-doped TiO_2 and N-doped TiO_2 samples were evaluated by monitoring oxidation of propylene

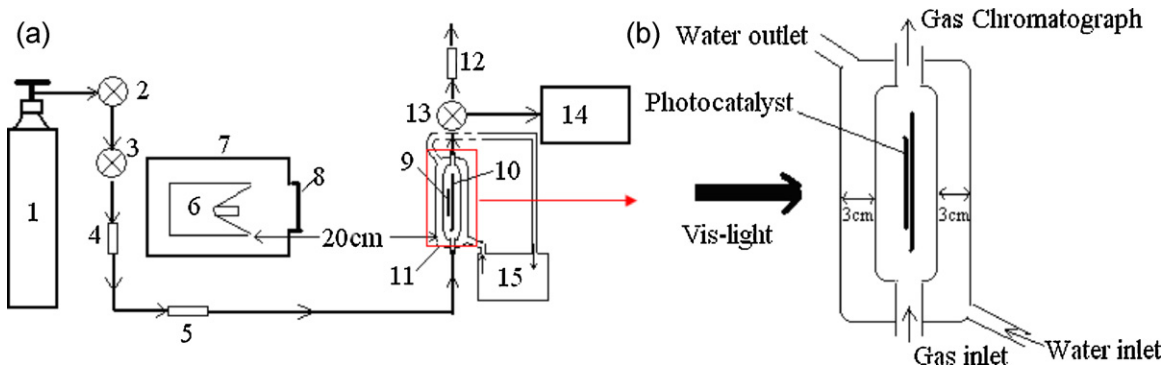

Fig. 1. Experimental equipment for photocatalytic oxidation of propylene (the red rectangle part in (a) is the home-made reactor, and its enlarged image is depicted in (b)). 1, feed gas cylinder; 2, gas regulator; 3, gas reset valve; 4, drying-tube (filled with anhyrous magnesium perchlorate); 5, chamber; 6, xenon lamp; 7, scaling ladder; 8, filter; 9, catalyst; 10, glass plate; 11, home-made reactor; 12, soap film flowmeter; 13, six-way valve; 14, gas chromatograph; 15, thermostatically recirculated water delivery. (For interpretation of the references to color in this figure legend, the reader is referred to the web version of this article.)

under visible light irradiation. The feed gas was made up of pure C_3H_6 (99.99%) and atmosphere and stored in a high-pressure cylinder. The flow rate of the feed gas was adjusted to 150 mL h^{-1}. The on-line concentration of C_3H_6, C, was determined at a sensitivity of 1 ppmV using a chromatograph (Shimadzu GC-9A) equipped with a flame ionization detector (FID), a GDX-502 column, and a reactor loaded with Ni catalyst for the methanization of CO_2. The removal rate of C_3H_6 was calculated as $(C_0 - C)/C_0 \times 100\%$; where C_0 refers to the initial C_3H_6 concentration (600 ppmV). About 20 mg of each sample was spread on one side of a roughened glass plate (ca. 10 cm^2) located in a flat quartz tube reactor. A 500 W xenon lamp was selected as the visible light source. Between the xenon lamp and reactor was inserted a cut filter ($\lambda \geq 420$ nm) to eliminate ultraviolet and retain visible light. The intensity of the light with $\lambda \geq 420$ nm irradiated on to-be-tested samples was ca. 3 mW/cm^2. Fig. 1a shows the detailed schematic diagram of evaluation system, while Fig. 1b depicts the home-made reactor. The reactor was surrounded by a 3-cm thick water channel so as to eliminate infrared light and keep a desirable reaction temperature by controlling water delivery. Furthermore, this makes it feasible to directly investigate the influence of infrared light on visible light photocatalytic activity of the catalysts by cutting off water delivery.

3. Results and discussion

3.1. Characterization of catalysts

3.1.1. Catalysts morphology and crystal structure

Typical TEM images of NTA-R, 3 wt.% Pt/TiO_2, NTA-I, and N-TiO_2-400 are shown in Fig. 2a–d, respectively. Both NTA-R (Fig. 2a) and NTA-I (Fig. 2c) have the same nanotubular morphology. This is in agreement with our previous results as reported elsewhere [8,43,44]. In the case of 3 wt.% Pt/TiO_2 samples (Fig. 2b), the nanotubular morphology kept almost unchanged after thermal treatment at 400 °C (in air for 3 h)/200 °C (in H_2 for 2 h). This maybe resulted from the supporting function of metallic Pt [45], while non-metallic N has no such function as shown in Fig. 2d. However, it should be noted that a part of samples were present in the form of nanoparticles, indicating that the nanotubular morphology of some NTA-R were broken to a certain extent. Furthermore, one could see that metallic Pt with particle size of 1–2 nm was well dispersed on the surface of TiO_2 (marked by arrows in Fig. 2b). In contrast, after thermal-treatment in flowing NH_3, the nanotubular morphology of NTA-I was transformed into nanoparticles for N-NTA-400 samples. The results were well in accordance with our previous paper that the NTA morphology were broken to form nanoparticles when treated at T = 400 °C in flowing NH_3, accompanying with the change of crystal form (from orthorhombic to anatase, discussed as below) [8].

The XRD patterns of both Pt-doped TiO_2 and N-doped TiO_2 samples are shown in Fig. 3a and b, respectively, where the inset in Fig. 3a demonstrates the structure pattern of NTA. NTA belongs to orthorhombic system in terms of crystal structure, which has been well elucidated elsewhere [43]. NTA is a thermally unstable material, both its nanotubular morphology and orthorhombic phase are easily changed under the post-heat-treatment temperature ≥400 °C [44]. As can be seen from Fig. 3a and b, both Pt-doped TiO_2 and N-doped TiO_2 samples displayed a single crystalline structure of anatase phase, whereas no rutile or other phases appeared, possibly because the post-heat-treatment temperature was not high enough for doped-TiO_2 to experience anatase–rutile phase transformation. The intensity of A (1 0 1) X-ray diffraction peak of Pt-doped TiO_2 samples is almost the same, meaning the same anatase crystallinity possibly due to the same post-heat-treatment temperature. In contrast, the increasing NH_3-heating temperature resulted in an increase in the intensity and sharpness of the anatase peaks accounting for their improved crystallinity of N-doped TiO_2 samples. This further proved that the degree of anatase crystallinity of relevant samples is closely related to the post-treatment-temperature. By comparison with the XRD patterns between 1 wt.% Pt/TiO_2 and N-TiO_2-400 (both have the same post-treatment-temperature at 400 °C), N-TiO_2-400 sample showed a much better anatase crystallinity than 1 wt.% Pt/TiO_2 sample, indicating that Pt-dopants species may hinder the crystals crystallization.

3.1.2. Defect analysis in TiO_2 matrix

Considering electron spin resonance (ESR) spectra as highly sensitive tool to study paramagnetic species in TiO_2 matrix, we have performed the ESR measurements of both Pt-doped TiO_2 and N-doped TiO_2 samples at room temperature in air and the results are shown in Fig. 4a and b, respectively. Precursor of NTA has no paramagnetic species accounting for there were free of ESR signals. However, as Fig. 4 displayed, an ESR signal with g = 2.004 was observed for all doped-samples, which has been assigned to the characteristics of single-electron-trapped oxygen vacancies (denoted as SETOVs). It has been well known that oxygen vacancies of TiO_2 can be obtained by way of reduction with H_2 or heat-treatment in vacuum [46–50]. However, the resultant oxygen vacancies are unstable against reoxidation. Naccache observed a symmetrical ESR signal with g = 2.003 on slightly reduced TiO_2 and attributed it to the localization of a conduction electron in the lattice [46]. Volodin detected an ESR signal with g = 2.004 for reduced anatase and ascribed it to the surface defects [47]. A sharp ESR

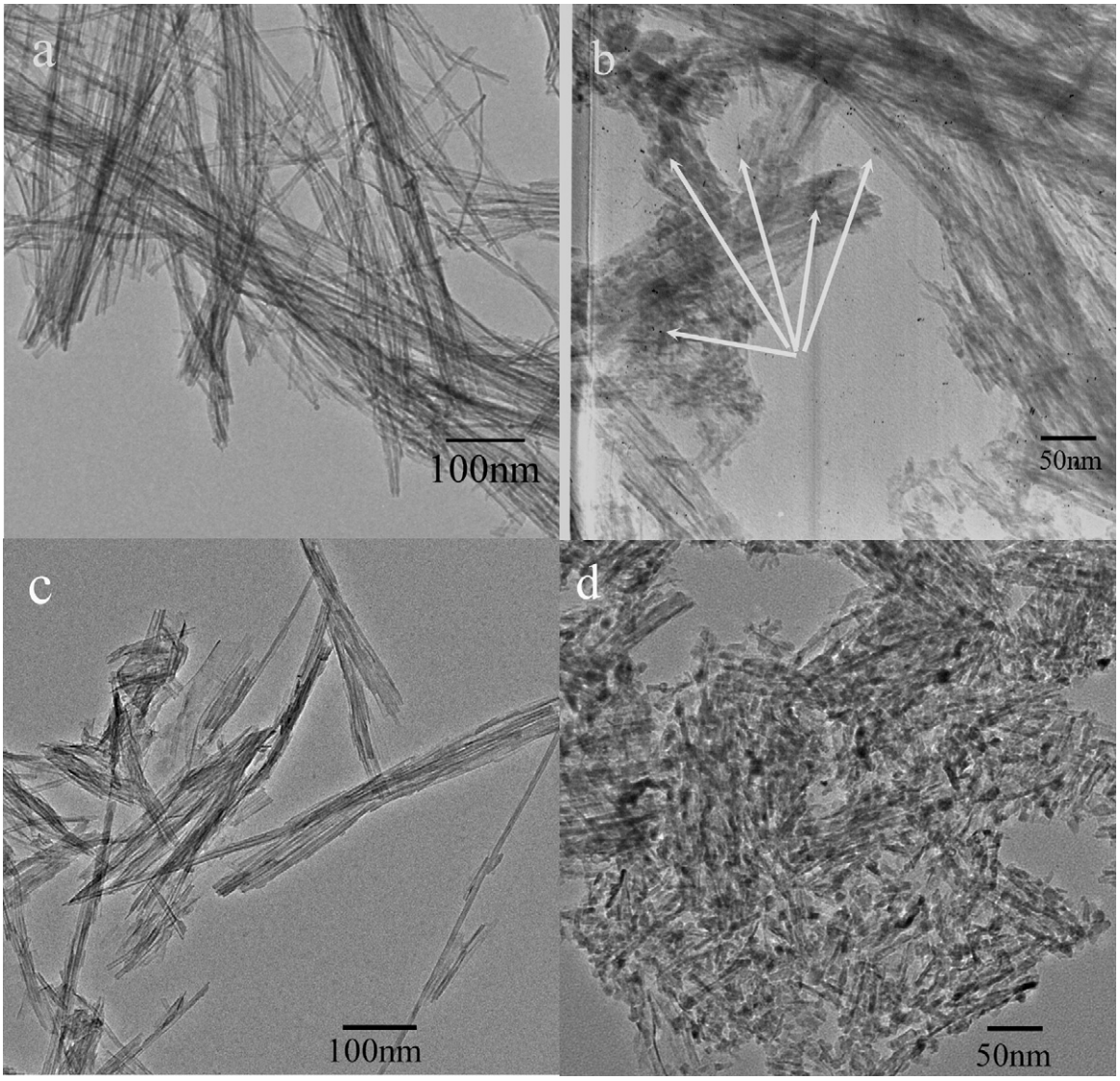

Fig. 2. Typical TEM images of (a) NTA-R, (b) 3 wt.% Pt/TiO_2, (c) NTA-I, and (d) N-TiO_2-400.

signal with $g = 2.003$ of TiO_2 after reduction in vacuum, registered at 77 K, was attributed to a bulk defect by Serwicka [48], probably an electron trapped on an oxygen vacancy, i.e., SETOVs. Ihara prepared a VLA TiO_2 photocatalyst by RF plasma treatment and observed the symmetrical ESR signal at $g = 2.003$ in the RF-plasma-heat-treated TiO_2 [49,50]. They assigned it to electrons trapped at oxygen-defect site, also can be denoted as SETOVs. Considering ammonia gas with weak alkalinity and liability to partly decompose

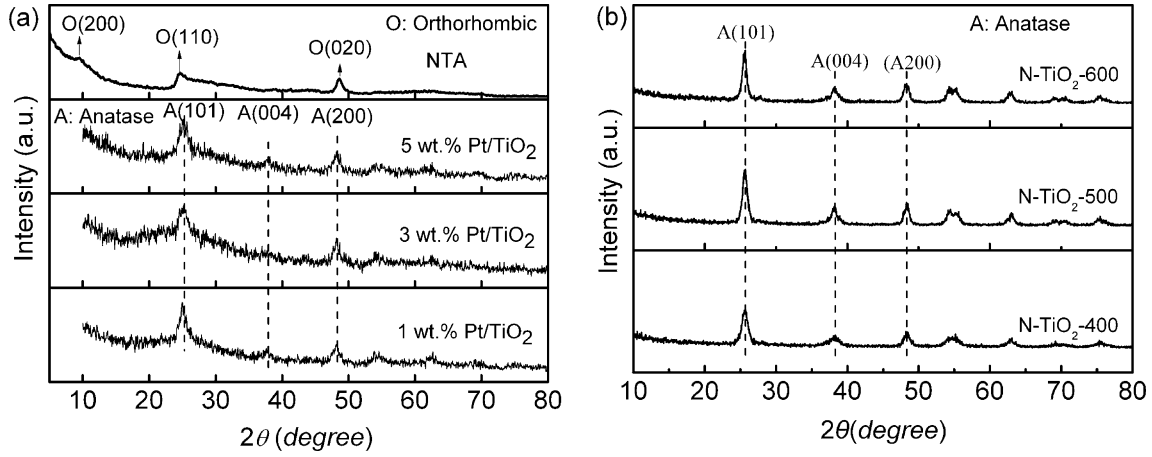

Fig. 3. XRD patterns of (a) NTA and Pt-doped TiO_2 and (b) N-doped TiO_2.

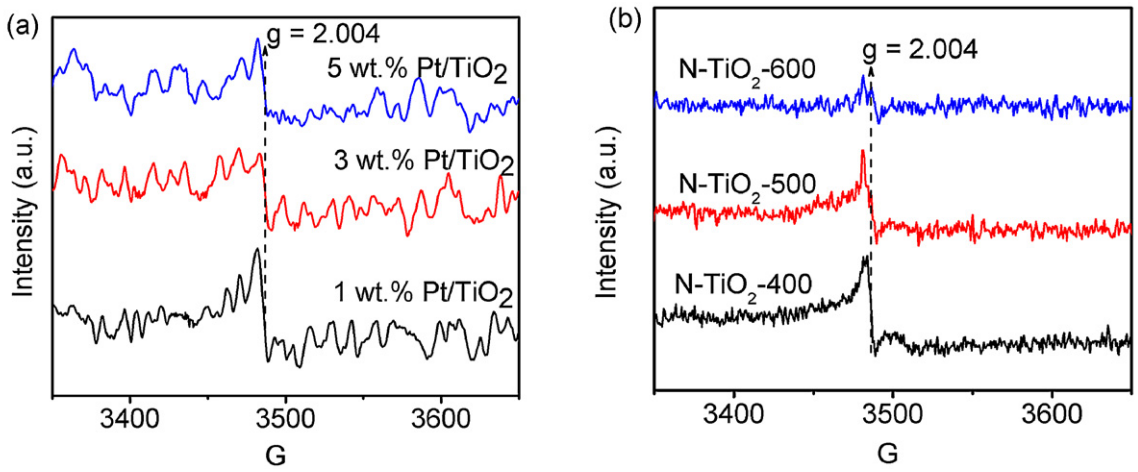

Fig. 4. ESR spectra of (a) Pt-doped TiO_2 and (b) N-doped TiO_2, measured at room temperature in atmosphere. The *g*-tensors of the ESR signals were obtained by setting *g* of diphenyl picryl hydrazyl (DPPH), 2.0036, as reference. ESR signal with $g = 2.004$ is the characterization of SETOVs in TiO_2 and the intensity of ESR signal is directly proportional to the concentration of SETOVs.

into H_2 and N_2, the NH_3-heat-treatment of NTA is hopefully to result in a slightly reduced N-doped TiO_2 whose $g = 2.004$ value ESR signal is assigned as SETOVs. As for the Pt-doped TiO_2 samples, H_2-reduction used in the post-treatment process can be expected to result in the formation of SETOVs. Factually, cation doping or anion doping into TiO_2 usually accompanies with the formation of defect in association with oxygen vacancies. On the one hand, for example, Li et al. prepared Ce-doped TiO_2 by a sol–gel process and proposed that the formation of oxygen vacancies energy level within bandgap may be one of critical reasons to reduce the recombination of electron–hole pairs and thus to enhance photocatalytic activity [51]. Choi et al. synthesized metal ions doped TiO_2 through sol–gel route and investigated the effect of individual dopants on the resulting physicochemical properties in association with visible light photocatalytic activities [52]. It was suggested that oxygen vacancies generated during synthesis contribute to the higher visible light photocatalytic activities of Pt–TiO_2 or Cr–TiO_2. On the other hand, as for the anion-doped TiO_2, Ihara et al. suggested that the visible light activity of N-doped TiO_2 arises from the oxygen vacancies caused by N doping [31]. Yu et al. prepared F-doped titania nanotubes and observed an increased photocatalytic activity due to the creation of oxygen vacancies and the presence of Ti^{3+} ions in the titania crystal structure [53]. Huang et al. obtained visible light response N–F-codoped TiO_2 by a sol–gel-solvothermal method and proposed that the doped N atoms can improve the visible light absorption, while the doped F atoms can facilitate the formation of oxygen vacancies, which are generally regarded as an important active species for initiating a photocatalytic reaction [54]. Recently, we prepared N-doped TiO_2 by annealing P25 or NTA in flowing NH_3 and evaluated their visible light photocatalytic activity toward oxidation of propylene and the relationship between SETOV and visible light photocatalytic activity was discussed in depth [40,41]. It was suggested that the visible light response of N-doped TiO_2 can be attributed to the formation of SETOVs, while N-dopants functions to prevent photoinduced electrons and holes from recombination. In the absence of either SETOVs in TiO_2 matrix or doped nitrogen on the surface, N-doped TiO_2 will not show visible light photocatalytic activity; and the higher the SETOVs concentration is, the better the visible light photocatalytic activity will be. Germane to the above discuss, we can conclude that the visible light sensitization of doped-TiO_2 is hardly excluded from the existence of oxygen vacancy.

Noticing that the intensity of ESR signal is directly proportional to the concentration of paramagnetic species, we can compare the intensity of the $g = 2.004$ ESR signal in relation to the concentration of SETOVs. As Fig. 4a shown, the concentration of SETOVs generated in Pt-doped TiO_2 samples containing different mass fractions of Pt kept almost unchanged, possibly due to the same post-heat-treatment. In contrast, N-doped TiO_2 samples possessed a gradually reduced concentration of SETOVs accompanying with the increase of post-heat-treatment temperature. However, N-doped TiO_2 even N-TiO_2-600 (it contains the lowest concentration of SETOVs among N-doped TiO_2 samples) still had a much higher concentration of SETOVs than that of Pt-doped TiO_2. This indicated that N-TiO_2-600 may have a higher visible light photocatalytic performance than Pt-doped TiO_2, and it was proved by the activity results discussed below.

3.2. XPS investigation

The surface chemical composition and chemical states of Pt- or N-doped TiO_2 samples analyzed by means of XPS are shown in Fig. 5, where the Pt 4*f*, Cl 2*p*, and N 1*s* XPS spectra are provided. Depending on the preparation procedure, Pt may exist as Pt(0), Pt(II) and/or Pt(IV). It can be seen from the deconvolution of Pt 4*f* spectra (inset in Fig. 5a) that Pt 4*f* signal consists of two typical doublet locating at around 71.1–74.4 eV and 72.3–75.6 eV, corresponding to metallic Pt(0) and oxidation Pt(II), respectively. The oxidation state of Pt often plays an important role on the enhancement of photocatalytic activity. Lee and Choi have reported that Pt(0) platinized TiO_2 has a better photocatalytic activity than Pt(II) platinized TiO_2 in terms of degradation of dichloroacetate, 4-chlorophenol and chloroform [14]. Teoh et al. systematically researched the inter-relationship between Pt oxidation states and the photocatalytic mineralization of organic matters [24]. It was suggested that formic acid-pretreated Pt/TiO_2 has a higher Pt(0) content than that of the as-prepared sample resulting in significantly higher rates of methanol mineralization due to the favorable interactions during photocatalytic reaction. Their results were in agreement with Mallat's view points that Pt(0) had beneficial effect in catalytic alcohol oxidation, where Pt_{ox} catalyst was known to be detrimental [55]. Hao et al. studied the catalytic oxidation of NO to NO_2 of Pt/TiO_2 catalysts prepared by wet impregnation and photodeposition method. Their experimental results showed that Pt(0)/TiO_2 prepared by impregnation exhibited quite higher activity than the sample Pt(II)/TiO_2 [56]. However, Wu et al. found that Pt(0)/TiO_2 and $PtCl_x$/TiO_2 had little contribution to the photocatalytic oxidation of NO in gas phase, while PtO_x/TiO_2 could

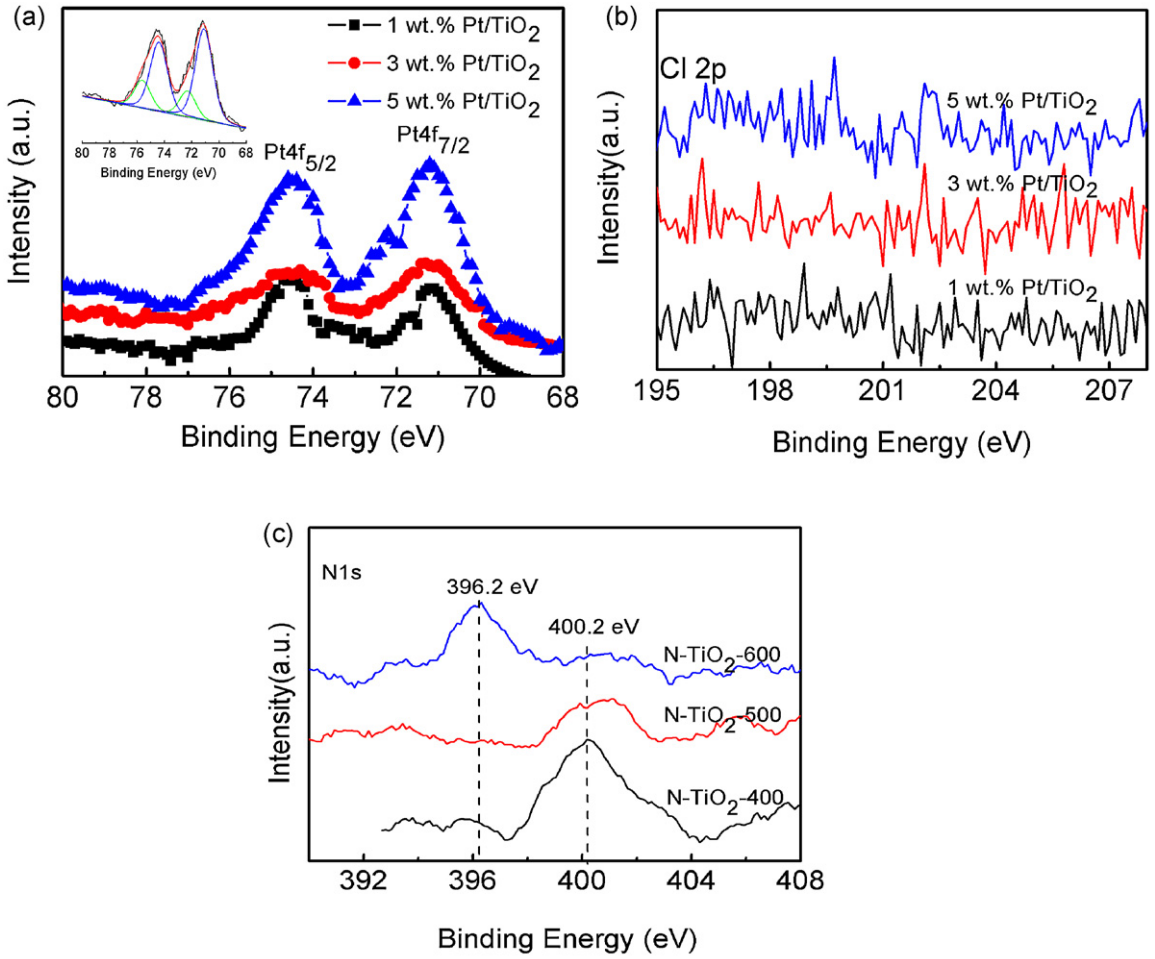

Fig. 5. XPS analysis of dopants of (a) Pt 4*f* XPS spectra of Pt-doped TiO_2, the inset displays its deconvolution spectrum, (b) Cl 2*p* XPS spectra of Pt-doped TiO_2, and (c) N 1*s* XPS spectra of N-doped TiO_2.

improve the NO photocatalytic oxidation efficiency and the reaction rate [57]. Huang et al. also observed that Pt(II)/TiO_2 with higher energy band gaps than metallic Pt(0)/TiO_2 showed a better water-splitting ability for H_2 production [58]. Based on the above discuss, it seems that the role of Pt oxidation states on photocatalytic activity is still vague. In the present paper, Pt(0) content is much more than Pt (II) content by comparison with their corresponding peak areas.

The Cl 2*p* XPS results recorded in Fig. 5b reveal that no chlorine elements were incorporated into TiO_2 matrix for all Pt-doped TiO_2 samples. This can be accounted for the decomposition of H_2PtCl_6 in air at certain temperature as follows [45]:

$$H_2Ti_2O_4(OH)_2 + H_2PtCl_6 + O_2 \rightarrow TiO_2 + PtO_x \quad (x = 0, 1) + H_2O + HCl\uparrow$$

where Cl elements were brought out in the form of gas HCl through volatilization. Although many papers have been available about the beneficial effect of chlorine sensitization of TiO_2 in enhancement of photocatalytic activity [59–62], the absence of Cl 2*p* signal presented in Fig. 5b indicated that the influence of chlorine element on visible light photocatalytic activity can be excluded.

Fig. 5c provides the N 1*s* XPS spectra of N-TiO_2-(400–600). No N 1*s* XPS signals were detected on the surface of NTA (figure is not given here). In terms of N-TiO_2-400 and N-TiO_2-500 samples, only a single N 1*s* XPS peak with a core level binding energy of 400.2 eV was observed, while as to sample N-TiO_2-600, an additional N species locating at the binding energy of 396.2 eV appeared except the weakened 400.2 eV signal. Usually the appearance of 396.2 eV XPS peak is considered as the evidence for the presence of Ti–N bonds formed when the nitrogen atoms replace the oxygen in the TiO_2 crystal lattice [63], while the assignment of 400.2 eV N species is still disputable. Namely, Asahi and co-workers reported three N 1*s* peaks with binding energies of 402 eV, 400 eV and 396 eV and assigned them as molecularly chemisorbed γ-N_2 (BE = 402 eV and 400 eV) and atomic β-N (BE = 396 eV) [27]. Such a chemisorption of molecular N_2 on N-doped TiO_2, nevertheless, was strongly argued by Sato and co-workers, who proposed that the N 1*s* species of N-doped TiO_2 at 400 eV should be ascribed as N–O bonding (i.e., Ti–O–N) [34]. This is seemingly more rational because molecular N_2 is not chemisorbed on metal oxides like TiO_2 at room temperature. Irie and co-workers assigned their N 1*s* peaks of N-doped TiO_2 at 400 eV and 396 eV as NO and TiN, respectively [28]. Li and co-workers prepared N-doped TiO_2 under supercritical conditions and observed two kinds of N species, O–Ti–N and surface adsorbed NH_3 molecules with a binding energy of 399.5 eV and 395.3 eV, respectively [64]. Suda and Fu et al. separately investigated their N 2*p* core line at 399.6 eV and suggested that it belongs to N–O structure of $TiO_{2-x}N_x$ [65,66]. Spadavecchia and co-workers synthesized nano-N-TiO_2 *via* a controlled sol–gel reaction followed by calcinations at 400 °C and ascribed their N 1*s* peak centered at ca. 399 eV to oxidized nitrogen (i.e., N–O–Ti–O species), possibly in interstitial location [67]. Kosowska and co-workers prepared N-doped TiO_2 catalysts by treating TiO_2 particles in gaseous NH_3 atmosphere for 4 h, almost the same route as ours but with different precursors [30]. Catalysts calcinated at 700 °C and 500/600 °C

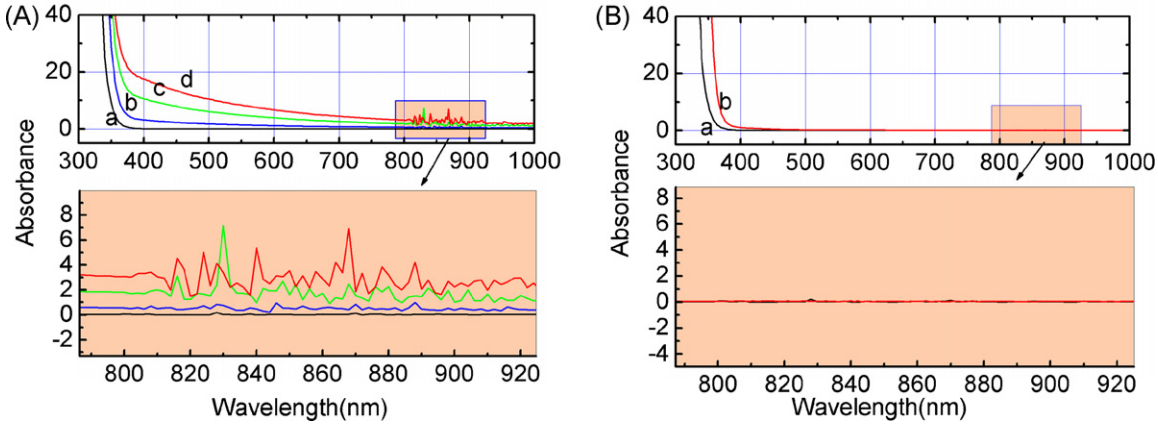

Fig. 6. UV–Vis–NIR spectra of (A) Pt-doped TiO_2: (a) P25, (b) 1 wt.% Pt/TiO_2, (c) 3 wt.% Pt/TiO_2, and (d) 5 wt.% Pt/TiO_2; (B) N-doped TiO_2: (a) P25 and (b) N-TiO_2-400.

showed the highest decomposition rate for phenol and azo-dye, respectively. However, they did not offer N 1*s* chemical state in their N-doped TiO_2 catalysts, nor did they explain the contribution of doped-N to the visible light sensitization. Considering that the chemical states of doped-N is still under controversy, we tend to assign the N 1*s* XPS peak of N-doped TiO_2 at 400.2 eV as Ti–O–N bonding, i.e., oxidized nitrogen. Moreover, the intensity of 400.2 eV signal was gradually decreased with the increase of temperature and 396.2 eV signal appeared for N-TiO_2-600 sample, indicating that the higher temperature was favorable to the formation of substitutional N species. This, in agreement with our previous results, is not surprise that even new TiN phase formed when the treatment temperature was adjusted to 700 °C [68]. It has been reported that the Ti–N bonds have a negative contribution to the visible light photocatalytic performance [35,67,68]. This, in agreement with the present results, can be confirmed by the activity tests of N-TiO_2 (see Fig. 8 below) in connect with the XPS results. It seems that the interstitial N species were more beneficial to activity improvement rather than substitutional N species.

3.3. *UV–Vis–NIR optical absorption spectra analysis*

Fig. 6 shows the UV–Vis–NIR spectra of P25-TiO_2 and doped-TiO_2 samples in the range of 300–1000 nm. It can be seen that the absorption threshold of Pt-doped TiO_2 is slightly red-shifted as compared to that of sample P25-TiO_2, accompanied with a gradually enhanced absorption around 400 nm due to the increase of Pt content. Many papers have explored the essence of visible light absorption of doped or undoped TiO_2. Jin and co-workers also ascribed the apparent visible light absorption of dehydrated NTA to the generation of SETOVs in crystal lattice [43]. Zhang and co-workers systematically studied the effect of annealing temperature on the morphology, structure and photocatalytic behavior of NTA and ascribed their apparent visible light absorption to the formation of SETOVs [44]. Besides, Yamada and co-workers attributed the visible light absorption to the formation of oxygen vacancies in association with removal of doped-N atoms from the particles during post-heat-treatment in air [69]. Based on a systematic analysis of the absorption spectral features of various titanium dioxide specimens, whether doped or undoped, in the visible spectral domain reported extensively in the literature, Serpone and co-workers suggested that the visible light absorption of TiO_2 was associated with oxygen vacancies (i.e., *F*-type color centers) [42]. Subsequently, Huang et al. offered a directly powerful proof that oxygen vacancies played a dominant role for visible-light absorption of TiO_2/MgO spheres, while MgO had no contribution to visible-light absorption. It seems dependable because no visible spectral response could be observed for the sample after calcination at 550 °C in air, due to the disappearance of oxygen vacancies after calcination [70]. Recently we also found that the visible light absorption of N-doped TiO_2 was proportional to the concentration of SETOVs [40,41]. In one word, it can be concluded that the visible light absorption of doped TiO_2 is originated from the generation of SETOVs. The above ESR results have indicated that the concentration of SETOVs generated in Pt-doped TiO_2 samples kept almost the same. This means that the visible light absorption of various Pt-doped TiO_2 samples, contributed by SETOVs, should be equal. Since the ability of visible light absorption of Pt-doped TiO_2 samples gradually increased with increasing the content of Pt, we can infer that Pt-dopants also favors the efficient utilize of visible light, which is in agreement with an added-optical absorption due to the presence of Pt as reported by Li et al. [66]. Namely, the visible light absorption of Pt-doped TiO_2 samples was co-determined by the synergistic effect between SETOVs and Pt. Interestingly, Pt-doped TiO_2 samples showed some absorption peaks within 800–900 nm, and the intensity of the absorption peaks increased with increasing the content of Pt; but samples P25-TiO_2 and N-doped TiO_2 had no such peaks (see Fig. 6B). Since the ESR results confirmed that N-doped TiO_2 had a much higher concentration of SETOVs than that of Pt-doped TiO_2, the absorption peaks in the range of 800–900 nm could not be resulted from the generation of SETOVs. In other words, such absorption peaks of Pt-doped TiO_2 samples may be closely related to their ability to absorb infrared light, since samples P25-TiO_2 and N-doped TiO_2 do not possess such ability. Indeed, platinum per se has unique optical properties and a large work function, leading to a large Schottky barrier at the metal–semiconductor heterojunction and hence allowing efficient trapping of photogenerated electrons (considering that Pt-doped TiO_2 samples were synthesized at 400 °C (in air) and 200 °C (in hydrogen), we can expect that they may contain Pt/TiO_2 heterojunction). This, in association with the strong interaction between Pt and TiO_2 under oxidizing or reducing atmosphere [71–75], may well account for the absorption peaks of Pt-doped TiO_2 samples in infrared light region. Namely, Sanchez and co-workers proposed an oxygen vacancy model to account generically for strong metal–support interaction. The generalized model was operative through the interaction of metal atoms with oxygen vacancies in oxide supports [71,72]. Xu and co-workers have performed an ab initio study of the effect of oxygen defect on the strong-metal–support interaction (SMSI) between Pt and TiO_2. It was suggested that Pt is preferentially adsorbed upon the oxygen vacant site on the TiO_2 [73]. Furthermore, Zhang and co-workers reported that when Pt/TiO_2 catalysts were calcinated at 673 K in air, the SMSI between Pt and TiO_2 occurred. Pt atoms on the surface could thermally diffuse into the lattice of TiO_2 grains

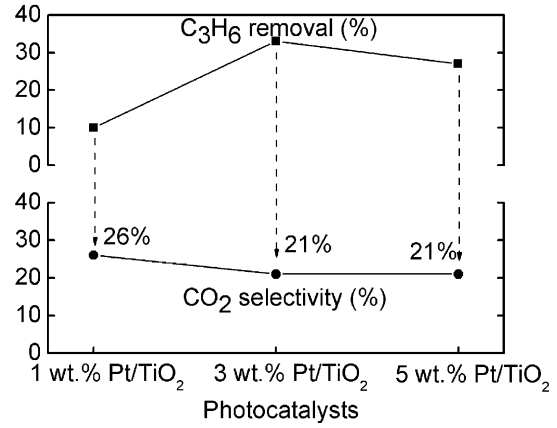

Fig. 7. Visible light photocatalytic activity toward oxidation of propylene accompanying with corresponding CO_2 selectivity of Pt-doped TiO_2 in the absence of infrared light participation.

[74,75], possibly located around oxygen vacancy site. Therefore, the electrons trapped in oxygen vacancies may easily transfer to the metallic Pt. Germane to this, absorption peaks within 800–900 nm could be interpreted as the result of the interaction between SETOV and noble metal Pt.

3.4. Visible light photocatalytic activity in the absence or the presence of infrared light irradiation

Samples NTA and P25-TiO_2 had no visible light photocatalytic activity for the photocatalytic oxidation of propylene. Fig. 7 shows the visible light photocatalytic activity of Pt-doped TiO_2 samples accompanying with corresponding CO_2 selectivity in the absence of infrared light irradiation (infrared light was eliminated by the water delivery) and the reaction temperature were maintained at room temperature. It can be seen that Pt-doped TiO_2 samples displayed an apparent visible light photocatalytic activity and 3 wt.% Pt/TiO_2 had a max propylene removal up to 33%. Unfortunately, the corresponding CO_2 selectivity that even the highest mineralization rate was only 26% for 1 wt.% Pt/TiO_2 were not perfect. As references, N-doped TiO_2 samples also showed an enhanced visible light photocatalytic activity as shown in Fig. 8. On the one hand, the visible light photocatalytic activities gradually decreased with increase of temperature and N-TiO_2-400 possessed the best photoactivity of 35%. On the other hand, the corresponding CO_2 selectivity that almost maintained unchanged at an average value

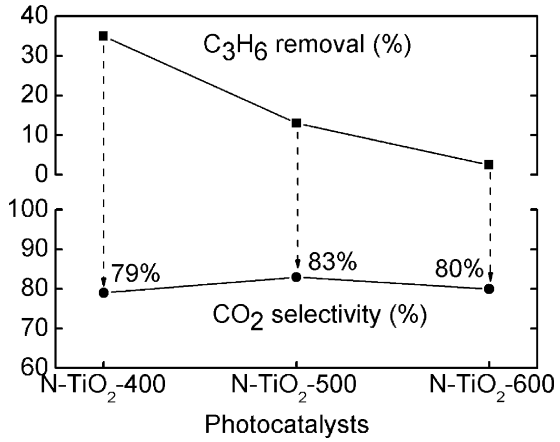

Fig. 8. Visible light photocatalytic activity toward oxidation of propylene accompanying with corresponding CO_2 selectivity of N-doped TiO_2 in the absence of infrared light participation.

of 81% were desirable. Both Pt-doped TiO_2 samples and N-doped TiO_2 samples cannot mineralize propylene completely into CO_2. There may be some intermediate products were not detected by gas chromatograph and also may be the methanization of CO_2 was not complete on the reactor loaded with Ni catalyst. By comparison with Pt-doped TiO_2 samples, N-TiO_2-400 possessed higher visible light photocatalytic activity and CO_2 selectivity than 3 wt.% Pt/TiO_2, indicating a stronger ability of oxidation propylene. It can be inferred that N-doped TiO_2 samples have more advantage in application of environmental purification if only used visible light source without infrared light photo-assistance.

In order to figure out the influence of infrared light on visible light photocatalytic activity, we performed the visible light photocatalytic activity by cutting off water delivery (see Fig. 1). This means that the infrared light was directly irradiated on the catalysts surface together with visible light. Fig. 9a shows the contrast between visible light photocatalytic activity of Pt-doped TiO_2 samples in the absence or the presence of additional infrared light irradiation. It is clear that Pt-doped TiO_2 samples have a giant enhancement in visible light photocatalytic activity of nearly 100% in the presence of infrared light irradiation (see curve B in Fig. 9a), noticeably differing from inertia or slightly increased photocatalytic activity of N-doped TiO_2 samples under the same condition (see Fig. 9b). Furthermore, the CO_2 selectivity of Pt-doped TiO_2 samples were simultaneously enhanced achieving to 80%, while it was unchanged for N-doped TiO_2 samples. This means that Pt-doped TiO_2 samples can utilize infrared light to greatly improve their visible light photocatalytic activity but N-doped TiO_2 samples not. This phenomenon, to the best of our knowledge, has not been reported elsewhere. Germane to this, Pt-doped TiO_2 can utilize the tails of solar light spectrum more efficiently than N-doped TiO_2, showing promising prospect in photocatalytic water splitting or/and environmental purification.

It has been reported that NTA has a band gap of 3.38 eV, corresponding to an absorption edge around 366 nm [76]. After doping with platinum or nitrogen in the presence of NTA as precursor, phase transformation from orthorhombic system to anatase occurs, accompanied with absorption threshold shifted to 387 nm accounting for the forbidden bandgap 3.2 eV of anatase. Photocatalytic reaction occurs only when photocatalyst is activated by absorbing light at a wavelength less than or equal to its exciton absorption wavelength. Since as-prepared samples are active beyond its absorption threshold ($\lambda \geq 420$ nm), their visible light sensitization should be originated from the intra-band energy offered by the formation of abundant SETOVs [40,41]. Dopants platinum or nitrogen functions not only to prevent photogenerated electrons and holes from recombination resulting in visible light photoactivity, but also to significantly increase visible light photocatalytic efficiency of the doped photocatalysts (see Fig. 6), resulting in the visible light photocatalytic activity. Both Pt-doped TiO_2 and N-doped TiO_2 samples have the same crystal structure of anatase phase (see Fig. 3), and N-doped TiO_2 samples possess a better crystallinity than that of Pt-doped TiO_2 samples. This means that the difference between the effect of infrared light on Pt-doped TiO_2 and N-doped TiO_2 cannot be elucidated by taking into account relevant XRD data. Similarly, the concentration of SETOVs also cannot be ascribed as the reason for the difference between the effect of infrared light on Pt-doped TiO_2 and N-doped TiO_2, since N-doped TiO_2 had a much higher concentration of SETOVs than that of Pt-doped TiO_2 but it is insusceptible to the infrared light.

The prerequisite condition for photoreactions is light excitation that results in photoinduced charges in association with the generation of active radical species. Can infrared light excite Pt-doped TiO_2 to generate more electrons and holes to participate the redox reaction resulting in the giant enhancement in visible light photocatalytic activity? Fig. 10 shows the visible light

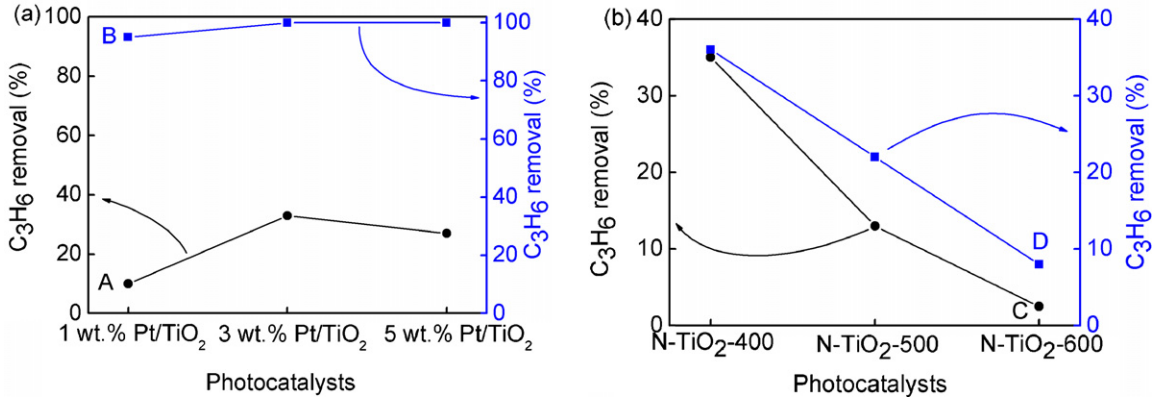

Fig. 9. Visible light photocatalytic activity toward oxidation of propylene of (a) Pt-doped TiO_2 and (b) N-doped TiO_2 before/after infrared light irradiation. Curves A and C in the absence of infrared light participation, B and D in the presence of infrared light participation. An intensive contrast between the effect of infrared light on the visible light photocatalytic activity was observed.

photocatalytic activity of 3 wt.% Pt/TiO_2 under light irradiation at a wavelength of $\lambda \geq 420$ nm, ≥460 nm, ≥490 nm, ≥510 nm and ≥550 nm in the absence or the presence of infrared light participation. The visible light photocatalytic activity of 3 wt.% Pt/TiO_2 gradually decreased with increasing irradiation wavelength, possibly due to the reduce of amount of excited photons therewith, whether in the absence or the presence of infrared light participation. Even so, 3 wt.% Pt/TiO_2 still possessed an enhanced visible light photocatalytic activity in the presence of infrared light irradiation. Nevertheless, whether photo-assisted by infrared light or not, it had almost no visible light photocatalytic activity when excited by light of $\lambda \geq 550$ nm. This implies that infrared light alone cannot excite 3 wt.% Pt/TiO_2 to photocatalyze propylene. Therefore, the photoreaction in the present system probably involves two processes. The first step is light excitation by visible light (light wavelength should be shorter than 550 nm), resulting in visible light photocatalytic activity. The second step is infrared light photo-assistance, resulting in a giant enhancement in visible light photocatalytic activity.

Considering that the infrared light has heating function, the reaction system temperature should be different before/after infrared light photo-assistance. Factually, it was measured that the reaction system temperature was warmed arriving at 110 °C from room temperature under infrared light irradiation. Therefore, it is necessary to find out the influence of reaction temperature on the photocatalytic activity of Pt-doped TiO_2 and N-doped TiO_2 so as to highlight on the difference between the effects of infrared light on the visible light photocatalytic activity. Fig. 11 shows the visible light photocatalytic degradation of propylene accompanying with CO_2 selectivity of 3 wt.% Pt/TiO_2 as a function of reaction temperatures in the absence of infrared light irradiation. With reaction temperature increasing, both the propylene removal and the CO_2 selectivity were gradually increased. The optical visible light photocatalytic activity along with CO_2 selectivity were obtained at temperature 110 °C up to 100% and 80%, respectively, which was warmed directly by infrared light through cutting off thermostatically recirculated water. It can be inferred that higher temperature was favorable to the visible light photocatalytic degradation of propylene of Pt-doped TiO_2. In contrast, the visible light photocatalytic activity together with CO_2 selectivity of N-TiO_2-400 seems to be regardless of the reaction temperature (see Fig. 12). When the reaction temperature was increased from 25 °C to 45 °C, the propylene degradation activity of N-TiO_2-400 was slightly increased, whereas the corresponding CO_2 selectivity maintained unchanged. Subsequently, the higher temperature resulted in the decrease in propylene degradation activity and reached a platforming photocatalytic activity, even at temperature 110 °C heated by infrared light irradiation. Alternatively, the corresponding CO_2 selectivity was almost the same regardless of reaction temperature. The intensive contrast between Pt-doped TiO_2 and N-doped TiO_2

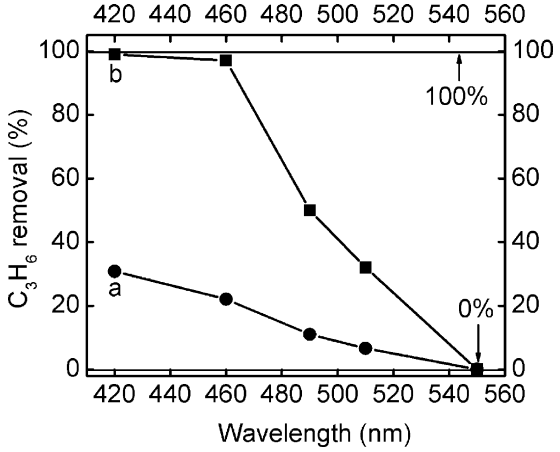

Fig. 10. Visible light photocatalytic activity of 3 wt.% Pt/TiO_2 under light irradiation at a wavelength of $\lambda \geq 420$ nm, ≥460 nm, ≥490 nm, ≥510 nm and ≥550 nm. Curve (a) in the absence of infrared light participation and (b) in the presence of infrared light participation.

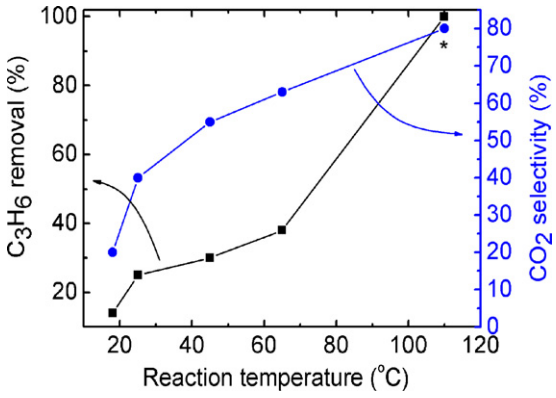

Fig. 11. Visible light photocatalytic degradation of propylene accompanying with CO_2 selectivity of 3 wt.% Pt/TiO_2 as a function of reaction temperatures in the absence of infrared light irradiation except * data. The reaction temperature <100 °C was controlled by controlling the temperature of thermostatically recirculated water. *Temperature was obtained in the presence of infrared light irradiation by cutting off thermostatically recirculated water.

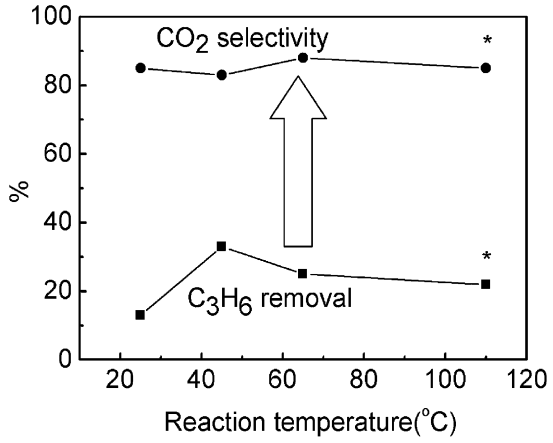

Fig. 12. Visible light photocatalytic degradation of propylene accompanying with CO_2 selectivity of N-TiO_2-400 as a function of reaction temperatures. The reaction temperature <100 °C was controlled by controlling the temperature of thermostatically recirculated water. *Temperature was obtained in the presence of infrared light irradiation by cutting off thermostatically recirculated water.

implied that reaction temperature may be closely related to the giant enhancement in visible light photocatalytic activity by additional infrared light irradiation for Pt-doped TiO_2 and the difference between the effect of infrared light on the visible light photocatalytic activity should be derived from the different characteristics of 3 wt.% Pt/TiO_2 and N-TiO_2-400. Namely, it is well known that platinum per se has unique optical properties and a large work function, leading to a large Schottky barrier at the metal–semiconductor heterojunction and hence allowing efficient trapping of photogenerated electrons. Considering that 3 wt.% Pt/TiO_2 samples were synthesized at 400 °C in air and 200 °C in hydrogen, we can expect that they may contain Pt/TiO_2 heterojunction. Furthermore, the existence of metallic Pt dopants on the surface of TiO_2 provides thermal catalytic sites [14–19]. In the presence of infrared light participation, the temperature around Pt/TiO_2 heterojunction is increased owing to the heating function of infrared light, this probably helps to accelerate the electron transfer and thus prevent charge recombination more effectively, and resulting in additional promoted visible light photocatalytic activity. However, as for N-doped TiO_2 samples, the characteristic surface structure of Pt-doped TiO_2 samples cannot be expected. This may be the really intrinsic origination accounting for the difference between the effect of infrared light on the visible light photocatalytic activity of Pt-doped TiO_2 and N-doped TiO_2.

4. Conclusions

Both Pt-doped TiO_2 and N-doped TiO_2 were prepared, using NTA as precursors, by wet impregnation and NH_3-heating method, respectively, aiming to compare the photocatalytic nature under visible light in the absence or the presence of infrared light participation. The visible light response was ascribed to the formation of SETOVs, while dopants elements functioned to prevent the photogenerated electrons and holes from recombination. N-doped TiO_2 showed a better visible light photocatalytic performance either in propylene degradation activity or in CO_2 selectivity than Pt-doped TiO_2 in the absence of infrared light. An intensive result showed that Pt-doped TiO_2 possessed a giant enhancement in visible light photocatalytic activity in the presence of additional infrared light participation, whereas N-doped TiO_2 seemed to be regardless of infrared light irradiation. Infrared light per se was unable to excite Pt-doped TiO_2 catalyst to initiate photocatalytic reaction. The strong interaction between platinum and oxygen vacancies resulted in infrared light absorption peaks at 800–900 nm, resulting in a giant enhancement in visible light photocatalytic activity of Pt-doped TiO_2 in the presence of infrared light irradiation. In contrast, samples N-doped TiO_2 do not possess such infrared light absorption peaks, which accounts for its visible light photodegradation of propylene immunizing from infrared light irradiation. The difference between the effect of reaction temperature on the visible light photocatalytic activity of Pt-doped TiO_2 and N-doped TiO_2 suggested that the influence of infrared light on visible light photocatalytic activity was derived from its heating function as well as dopants platinum act as thermal catalysis cites. Moreover, the intrinsic Pt/TiO_2 heterojunctions are benefit to the photoinduced electrons transfer and then captured by oxygen to produce superoxide or other active species resulting in apparent visible light photocatalytic activity. In the presence of infrared light participation, the temperature around Pt/TiO_2 heterojunction was increased owing to the absorption of infrared light, which helped to accelerate the electron transfer and prevent charge recombination more effectively, resulting in additional improvement of visible light photocatalytic activity. It could be concluded that Pt-doped TiO_2 can utilize the tails of solar light spectrum more efficiently than N-doped TiO_2, showing promising prospect in photocatalytic water splitting or/and environmental purification.

References

[1] H.M. Luo, T. Takata, Y. Lee, J.F. Zhao, K. Domen, Y.S. Yan, Chem. Mater. 16 (2004) 846–849.
[2] A. Kudo, Y. Miseki, Chem. Soc. Rev. 38 (2009) 253–278.
[3] Q. Xu, Y. Ma, J. Zhang, X.L. Wang, Z.C. Feng, C. Li, J. Catal. 278 (2011) 329–335.
[4] L.F. Qi, J.G. Yu, M. Jaroniec, Phys. Chem. Chem. Phys. 13 (2011) 8915–8923.
[5] J. Zhang, Q. Xu, Z.C. Feng, M.J. Li, C. Li, Angew. Chem. Int. Ed. 47 (2008) 1766–1769.
[6] O.K. Varghese, M. Paulose, T.J. LaTempa, C.A. Grimes, Nano Lett. 9 (2009) 731–737.
[7] C.J. Wang, R.L. Thompson, J. Baltrus, C. Matranga, J. Phys. Chem. Lett. 1 (2009) 48–53.
[8] Y. Wang, C.X. Feng, Z.S. Jin, J.W. Zhang, J.J. Yang, S.L. Zhang, J. Mol. Catal. A: Chem. 260 (2006) 1–3.
[9] B.Z. Tian, C.Z. Li, F. Gu, H.B. Jiang, Catal. Commun. 10 (2009) 925–929.
[10] M. Bellardita, M. Addamo, A. Di Paola, L. Palmisano, A. Venezia, Phys. Chem. Chem. Phys. 11 (2009) 4084–4093.
[11] F. Chen, W.W. Zou, W.W. Qu, J.L. Zhang, Catal. Commun. 10 (2009) 1510–1513.
[12] V. Etacheri, M.K. Seery, S.J. Hinder, S.C. Pillai, Chem. Mater. 22 (2010) 3843–3853.
[13] X.B. Chen, S.S. Mao, Chem. Rev. 107 (2007) 2891–2959.
[14] J. Lee, W. Choi, J. Phys. Chem. B 109 (2005) 7399–7406.
[15] H. Park, J. Lee, W. Choi, Catal. Today 111 (2006) 259–265.
[16] W. Zhao, C.C. Chen, X.Z. Li, J.C. Zhao, H. Hidaka, N. Serpone, J. Phys. Chem. B 106 (2002) 5022–5028.
[17] S. Hwang, M.C. Lee, W. Choi, Appl. Catal. B: Environ. 46 (2003) 49–63.
[18] S. Kim, W. Choi, J. Phys. Chem. B 106 (2002) 13311–13317.
[19] H. Haick, Y. Paz, J. Phys. Chem. B 107 (2003) 2319–2326.
[20] V. Keller, P. Bernhardt, F. Garin, J. Catal. 215 (2003) 129–138.
[21] S. Sakthivel, M. Shankar, M. Palanichamy, B. Arabindoo, D. Bahnemann, V. Murugesan, Water Res. 38 (2004) 3001–3008.
[22] A. Vorontsov, I. Stoyanova, D. Kozlov, V. Simagina, E. Savinov, J. Catal. 189 (2000) 360–369.
[23] F. Denny, J. Scott, K. Chiang, W.Y. Teoh, R. Amal, J. Mol. Catal. A: Chem. 263 (2007) 93–102.
[24] W.Y. Teoh, L.M. dler, R. Amal, J. Catal. 251 (2007) 271–280.
[25] C.A. Emilio, I. Marta, M. Kunst, M. Bouchard, C. Colbeau-Justin, Langmuir 22 (2006) 3606–3613.
[26] F.B. Li, X.Z. Li, Chemosphere 48 (2002) 1103–1111.
[27] R. Asahi, T. Morikawa, T. Ohwaki, K. Aoki, Y. Taga, Science 293 (2001) 269–271.
[28] H. Irie, Y. Watanabe, K. Hashimoto, J. Phys. Chem. B 107 (2003) 5483–5486.
[29] O. Diwald, T.L. Thompson, T. Zubkov, E.G. Goralski, S.D. Walck, J.T. Yates Jr., J. Phys. Chem. B 108 (2004) 6004–6008.
[30] B. Kosowska, S. Mozia, A.W. Morawski, B. Grzmil, M. Janus, K. Kalucki, Sol. Energy Mater. Sol. Cells 88 (2005) 269–280.
[31] T. Ihara, M. Miyoshi, Y. Iriyama, O. Matsumoto, S. Sugihara, Appl. Catal. B: Environ. 42 (2003) 403–409.
[32] J. Ananpattarachai, P. Kajitvichyanukul, S. Seraphin, J. Hazard. Mater. 168 (2009) 253–261.
[33] S.Z. Hu, A.J. Wang, X. Li, H. Löwe, J. Phys. Chem. Solids 71 (2010) 156–162.
[34] S. Sato, R. Nakamura, S. Abe, Appl. Catal. A: Gen. 284 (2005) 131–137.
[35] O. Diwald, T.L. Thompson, E.G. Goralski, S.D. Walck, J.T. Yates Jr., J. Phys. Chem. B 108 (2004) 52–57.

[36] A. Ghicov, J.M. Macak, H. Tsuchiya, J. Kunze, V. Haeublein, L. Frey, P. Schmuki, Nano Lett. 6 (2006) 1080–1082.
[37] A. Ghicov, J.M. Macak, H. Tsuchiya, J. Kunze, V. Haeublein, S. Kleber, P. Schmuki, Chem. Phys. Lett. 419 (2006) 426–429.
[38] R. Vitiello, J. Macak, A. Ghicov, H. Tsuchiya, L. Dick, P. Schmuki, Electrochem. Commun. 8 (2006) 544–548.
[39] T. Morikawa, R. Asahi, T. Ohwaki, K. Aoki, Y. Taga, Jpn. J. Appl. Phys. 40 (2001) 561–563.
[40] Y. Wang, C.X. Feng, M. Zhang, J.J. Yang, Z.J. Zhang, Appl. Catal. B: Environ. 100 (2010) 84–90.
[41] Y. Wang, C.X. Feng, M. Zhang, J.J. Yang, Z.J. Zhang, Appl. Catal. B: Environ. 104 (2011) 268–274.
[42] V.N. Kuznetsov, N. Serpone, J. Phys. Chem. C 113 (2009) 15110–15123.
[43] S.L. Zhang, W. Li, Z.S. Jin, J.J. Yang, J.W. Zhang, Z.L. Du, Z.J. Zhang, J. Solid State Chem. 177 (2004) 1365–1371.
[44] M. Zhang, Z.S. Jin, J.W. Zhang, X.Y. Guo, J.J. Yang, W. Li, X.D. Wang, Z.J. Zhang, J. Mol. Catal. A: Chem. 217 (2004) 203–210.
[45] C.X. Feng, Z.S. Jin, X.D. Wang, J.J. Yang, Photogr. Sci. Photochem. 25 (2007) 12–17.
[46] C. Naccache, P. Meriaudeau, M. Che, A. Tench, Trans. Faraday Soc. 67 (1971) 506–512.
[47] A. Volodin, A. Cherkashin, V. Zakharenko, React. Kinet. Catal. Lett. 11 (1979) 107–111.
[48] E. Serwicka, Colloids surf. 13 (1985) 287–293.
[49] K. Takeuchi, I. Nakamura, O. Matsumoto, S. Sugihara, M. Ando, T. Ihara, Chem. Lett. 29 (2000) 1354–1355.
[50] T. Ihara, M. Miyoshi, M. Ando, S. Sugihara, Y. Iriyama, J. Mater. Sci. 36 (2001) 4201–4207.
[51] F.B. Li, X.Z. Li, M.F. Hou, K.W. Cheah, W.C.H. Choy, Appl. Catal. A: Gen. 285 (2005) 181–189.
[52] J. Choi, H. Park, M.R. Hoffmann, J. Phys. Chem. C 114 (2009) 783–792.
[53] Y. Yu, H.H. Wu, B.L. Zhu, S.R. Wang, W.P. Huang, S.H. Wu, S.M. Zhang, Catal. Lett. 121 (2008) 165–171.
[54] D.G. Huang, S.J. Liao, J.M. Liu, Z. Dang, L. Petrik, J. Photochem. Photobiol. A: Chem. 184 (2006) 282–288.
[55] T. Mallat, A. Baiker, Catal. Today 19 (1994) 247–283.
[56] L.D. Li, Q. Shen, J. Cheng, Z.P. Hao, Appl. Catal. B: Environ. 93 (2010) 259–266.
[57] H.Q. Wang, Z.B. Wu, Y. Liu, Y.J. Wang, Chemosphere 74 (2009) 773–778.
[58] B.S. Huang, F.Y. Chang, M.Y. Wey, Int. J. Hydrogen Energy 35 (2010) 7699–7705.
[59] W. Macyk, H. Kisch, Chem. Eur. J. 7 (2001) 1862–1867.
[60] W. Zhao, C.C. Chen, W.H. Ma, J.C. Zhao, D.X. Wang, H. Hidaka, N. Serpone, Chem. Eur. J. 9 (2003) 3292–3299.
[61] K. Hashimoto, K. Sumida, S. Kitano, K. Yamamoto, N. Kondo, Y. Kera, H. Kominami, Catal. Today 144 (2009) 37–41.
[62] C.H. Huang, I.K. Wang, Y.M. Lin, Y.H. Tseng, C.M. Lu, J. Mol. Catal. A: Chem. 316 (2010) 163–170.
[63] N.C. Saha, H.G. Tompkins, J. Appl. Phys. 72 (1992) 3072–3079.
[64] H.X. Li, J.X. Li, Y.N. Huo, J. Phys. Chem. B 110 (2006) 1559–1565.
[65] Y. Suda, H. Kawasaki, T. Ueda, T. Ohshima, Thin Solid Films 453 (2004) 162–166.
[66] D.Z. Li, Z.X. Chen, Y.L. Chen, W.J. Li, H.J. Huang, Y.H. He, X.Z. Fu, Environ. Sci. Technol. 42 (2008) 2130–2135.
[67] F. Spadavecchia, G. Cappelletti, S. Ardizzone, C.L. Bianchi, S. Cappelli, C. Oliva, P. Scardi, M. Leoni, P. Fermo, Appl. Catal. B: Environ. 96 (2010) 314–322.
[68] C.X. Feng, Y. Wang, Z.S. Jin, J.W. Zhang, S.L. Zhang, Z.S. Wu, Z.J. Zhang, New J. Chem. 32 (2008) 1038–1047.
[69] K. Yamada, H. Yamane, S. Matsushima, H. Nakamura, K. Ohira, M. Kouya, K. Kumada, Thin Solid Films 516 (2008) 7482–7487.
[70] X.J. Lu, F.Q. Huang, J.J. Wu, S.J. Ding, F.F. Xu, ACS Appl. Mater. Interfaces 3 (2011) 566–572.
[71] M. Spencer, J. Catal. 93 (1985) 216–223.
[72] M. Sanchez, J. Gazquez, J. Catal. 104 (1987) 120–135.
[73] X. Wei-Xing, K. Schierbaum, W. Goepel, J. Solid State Chem. 119 (1995) 237–245.
[74] M. Zhang, Z.S. Jin, Z.J. Zhang, H.X. Dang, Appl. Surf. Sci. 250 (2005) 29–34.
[75] Q.Y. Li, K. Wang, S.L. Zhang, M. Zhang, J.J. Yang, Z.S. Jin, J. Mol. Catal. A: Chem. 258 (2006) 83–88.
[76] E. Morgado Jr., B.A. Marinkovic, P.M. Jardim, M.A.S. de Abreu, F.C. Rizzo, J. Solid State Chem. 182 (2009) 172–181.